www.sciencemag.org/cgi/content/full/314/5806/1735/DC1

Supporting Online Material for

Mineralogy and Petrology of Comet 81P/Wild 2 Nucleus Samples

Michael E. Zolensky,* Thomas J. Zega, Hajime Yano, Sue Wirick, Andrew J. Westphal, Mike K. Weisberg, Iris Weber, Jack L. Warren, Michael A. Velbel, Akira Tsuchiyama, Peter Tsou, Alice Toppani, Naotaka Tomioka, Kazushige Tomeoka, Nick Teslich, Mitra Taheri, Jean Susini, Rhonda Stroud, Thomas Stephan, Frank J. Stadermann, Christopher J. Snead, Steven B. Simon, Alexandre Simionovici, Thomas H. See, François Robert, Frans J.M. Rietmeijer, William Rao, Murielle C. Perronnet, Dimitri A. Papanastassiou, Kyoko Okudaira, Kazumasa Ohsumi, Ichiro Ohnishi, Keiko Nakamura-Messenger, Tomoki Nakamura, Smail Mostefaoui, Takashi Mikouchi, Anders Meibom, Graciela Matrajt, Matthew A. Marcus, Hugues Leroux, Laurence Lemelle, Loan Le, Antonio Lanzirotti, Falko Langenhorst, Alexander N. Krot, Lindsay P. Keller, Anton T. Kearsley, David Joswiak, Damien Jacob, Hope Ishii, Ralph Harvey, Kenji Hagiya, Lawrence Grossman, Jeffrey N. Grossman, Giles A. Graham, Matthieu Gounelle, Philippe Gillet, Matthew J. Genge, George Flynn, Tristan Ferroir, Stewart Fallon, Denton S. Ebel, Zu Rong Dai, Patrick Cordier, Benton Clark, Miaofang Chi, Anna L. Butterworth, Donald E. Brownlee, John C. Bridges, Sean Brennan, Adrian Brearley, John P. Bradley, Pierre Bleuet, Phil A. Bland, Ron Bastien

*To whom correspondence should be addressed. E-mail: michael.e.zolensky@nasa.gov

Published 15 December 2006, *Science* **314**, 1735 (2006)
DOI: 10.1126/science.1135842

This PDF file includes:

Supporting Online Material

Techniques

A fuller description of the Stardust tracks described in this paper is given in the online Stardust Sample Catalog (*S1*). This Catalog is constantly being updated with data for newly analyzed Tracks.

To remove grains from aerogel we used a combination of old and new techniques. For larger features we could use straight razor blades to trim away excess aerogel. For the bulk of tracks however, we mainly used two newly-developed techniques: keystoning and quikstoning (Fig. S6).

Whole tracks in the aerogel collectors were extracted using the keystoning technique developed at the Space Sciences Laboratory, U. C. Berkeley (*S2*). Glass rods (1mm diameter) are pulled to make two microneedles. The needles are held by micromanipulators which are attached to the stage of the extraction microscope. The needles cut the aerogel by repetitive "poking". The micromanipulators are driven automatically by computer. First, an angled cut is made which undercuts the deepest feature of a particular impact; then a vertical cut is made around the impact. The resulting wedge-shaped block of aerogel (a "keystone") contains the entire impact track and the terminal particles. The keystone is then removed from the collector using silicon microforks which are inserted into pre-machined holes in the keystone. For certain analytical techniques, it is desirable to slice a track into multiple cross-sections; other techniques require a sample of the bulb that has been cleaved lengthwise. These specialized samples are prepared by laying a keystone on its side and using the same aerogel cutting tools to dissect or slice wafers of the track bulb. Some analyses can be made of grains still enclosed in a suitably

small keystone, for example synchrotron X-ray diffraction (XRD) and X-ray fluorescence (XRF). When it is time to extract grains from the keystone it can be flattened between two sheets of mylar, and the grains can be easily separated. The flattened keystone preserves the general positions of the enclosed grains, permitting surveys to be made of mineralogical variation down tracks. For Stardust samples, we made keystones at University of California, Berkeley, and at the NASA Johnson Space Center (JSC) (*S1*).

In quikstoning, a diamond, steel or sapphire utility-knife-shaped blade is driven through the aerogel at ultrasonic frequencies. This micro-blade is controlled by a micromanipulator for fine motion control. The ultrasonic oscillations are generated by the piezo-driver of a MicroDissector (Eppendorf) which is mounted on the micromanipulator. Details of the instrument are given in (*S3*). Quikstoning was performed at the Lawrence Livermore National Lab and NASA JSC.

The embedding media for Wild 2 grains were EMBED-812 epoxy, sulfur and WELD-ON 40 acrylic. We most frequently used acrylic to mount grains for ultramicrotomy. Particles could then be easily removed from the embedding medium using common organic solvents, including acetone or chloroform, permitting subsequent isotopic or bulk compositional analyses. One problem we encountered was that acrylic polymerized in an electron beam, making subsequent grain removal difficult. We embedded pieces of aerogel in EMBED-812 epoxy, during which the aerogel became completely invisible, revealing all of the grains in a track in the most complete manner (*S4*). When it was desirable to make superior organic analyses of grains following ultramicrotomy we used sulfur as the embedding medium, as had been the standard practice for IDPs and fine-grained chondritic meteorites.

Comet Wild 2 grains were also embedded in high-purity S and sliced into 50~ 70 nm-thick sections with an ultramicrotome equipped with a diamond knife. The sections were floated onto ultra-pure water and transferred to amorphous C-supported Cu Transmission Electron Microscopy (TEM) grids. The S was sublimed prior to analysis focused on organic matter in the sample such as C- and N- X-ray Absorption Near-Edge Structure (XANES), Fourier Transform Infra-Red spectroscopy (FTIR) and light element isotopic analysis in the Nano- Secondary Ion Mass Spectrometer (NanoSIMS). Sulfur was chosen as an embedding medium to avoid contamination of the samples with low viscosity resin (epoxy) normally used for ultramicrotomy. Sulfur beads containing the samples were attached to a sample holding bullet using cyanoacrylate. To evaluate the potential glue contribution to the sample analysis, sulfur beads devoid of sample were prepared in the same manner. We did not see any evidence that cyanoacrylate penetrated the S bead during subsequent TEM investigation of the sample-free S slices. Electron Energy-Loss Spectroscopy (EELS) spectra acquired from the S test slices also did not show evidence of the pronounced CN peak characteristic of cyanoacrylate.

Micro-FTIR was used to provide a rapid, non-destructive pre-characterization of most grains removed from the aerogel at JSC. This technique was most valuable for terminal grains, which typically contained crystals larger than 1 um. However, FTIR generally failed to locate crystalline material within finer-grained particles, especially those from the upper portions (including bulbs) of tracks.

For Synchrotron X-ray Powder Diffraction (SXRF) each particle was mounted on a thin glass fiber with a 3 μm thickness using a small amount acetone-soluble bond, set in a Gandolfi camera, and exposed to synchrotron X-rays with a wave length of 2.161 ± 0.001 Å for 3 hours to produce a powder X-ray diffraction pattern. The analysis was performed at beam line 3A of the

Photon Factory, Institute of Material Science, High Energy Accelerator Research Organization and at beam line 37XU of the Japan Synchrotron Radiation Research Institute (SPring 8).

The TEM results reported have been obtained at many institutions. In Lille we used a Philips CM30 (LaB6 filament, working at 300 keV) and a Tecnai G2-20 twin (LaB6 filament, 200 kV). Structural (diffraction) data were obtained using the Selected Area Electron Diffraction (SAED) technique. Chemical compositions were measured using Energy Dispersion X-ray Spectroscopy (EDX) Noran and EDX Si-detectors (CM30 and Tecnai, respectively). Correction procedures have been applied (k-factors and absorption corrections).

At Michigan State University we used a JEOL 6400 Scanning Electron Microscope (SEM) operated at 25kV, with a Noran EDX system. TEM work here was performed using a JEOL 2200FS Field Emission Gun (FEG) TEM at 200kV, with an Oxford EDX system.

At Kobe University grains were studied using a TEM (JEOL JEM-2010) operated at 200 kV and equipped with an EDX detector For quantitative TEM analyses, k-factors for the major elements were determined using standards of San Carlos olivine, San Carlos clinopyroxene, and K-feldspar from Koryu mine, Hokkaido, Japan.

At Friedrich-Schiller-University Jena we used an energy-filtered 200 kV ZEISS LEO922 TEM with a ThermoNoran Six EDX system.

At the University of Chicago, samples were examined with a JEOL JSM-5800 low voltage SEM equipped with an Oxford/Link ISIS-300 EDX system. We also used a Tecnai F30 TEM, with a point-to-point resolution of 0.2 nm, operated at 300 kV.

At the University of New Mexico all STARDUST analyses were performed using a JEOL GEM2010 High Resolution TEM with point-to-point resolution of 0.19 nm. It is equipped with a LINK ISIS EDX system for in situ element analyses with a 5 nm probe. The spectrometer

is fitted with an ultrathin window for quantitative light element analyses. The instrument operated at a 200keV accelerating voltage. Additional analyses were performed using a JEOL 2010F FASTEM TEM/STEM instrument operating at 197 keV. The instrument is equipped with a GATAN GIF 2000 imaging filtering system and Oxford INCA/Isis EDS system. The Cliff-Lorimer thin-film procedure was used for quantitative chemical determination with an error <10% (relative). Crystallographic data were obtained by SAED. An LN2-cooled cold-finger was used to minimize sample degradation. Each sample was placed in low-background double-tilt sample holder that was dedicated to this particular project to avoid contact with extraneous materials. All sample handling occurred inside a laminar flow bench.

At the Naval Research Lab TEM analyses were performed using a JEOL 2200FS 200 kV field-emission microscope equipped with a Noran System Six EDX and Gatan Ultrascan Charge-Coupled Device (CCD).

At Tokyo University we used a Hitachi S-4500 FEG-SEM with EDX and Electron Back-Scattered Diffraction (EBSD). We also used a JEOL JEM2010 TEM with an EDX system.

TEM measurements at NASA Johnson Space Center were obtained using a JEOL 2500SE 200kV FEG-STEM equipped with a Noran thin window EDX spectrometer, a Gatan Tridiem imaging filter for Energy-Filtered TEM imaging (EFTEM) and EELS, and a 2K x 2K slow scan CCD camera for recording images. Image acquisition and processing were carried out using Gatan Digital Micrograph software. EFTEM images were collected with acquisition times of 20-60 s depending on element concentrations. EELS spectra were obtained in image mode with spot sizes of 10-50 nm, a dispersion of 0.3 eV, dwell times of 10-30 s at an energy resolution of 0.9 eV full width half maximum at the zero-loss peak. High resolution brightfield

images were recorded at 500K-1M X magnification and ordering was estimated using fast Fourier transforms of selected regions within the images.

Time-of-Flight Secondary Ion Mass Spectrometry (TOF-SIMS) was used to obtain lateral element distributions of eight particles sectioned in epoxy as well as two tracks on dissected aerogel keystones. A TOF-SIMS IV instrument from ION-TOF was used in this study. TOF-SIMS allows a comprehensive analysis of elements, isotopes, and molecules at high lateral resolution and minute sample consumption. During a typical TOF-SIMS analysis, less than one atomic monolayer is consumed while the sample is bombarded with a pulsed 25 keV Ga^+ primary ion beam for several hours. This beam with a diameter of ~0.2 µm is rastered over the sample to obtain information on the lateral distribution of the various elements, isotopes, and molecules. All secondary ions of a single polarity are detected quasi simultaneously after their passage through the time-of-flight spectrometer. Both polarities are measured in two consecutive analyses. Further details on the TOF-SIMS technique are given in the literature (*S5*).

Three-dimensional structures of four particles which had been measured by SXRD were obtained non-destructively using Synchrotron micro-tomography. The imaging experiments were performed at beam line BL 47XU of SPring-8. This imaging tomographic technique (*S6*) was applied to obtain the pixel size of 42.5 nm, which gives an effective spatial resolution below a few hundred nm. The X-ray energy was 8 keV. About 500-700 successive CT images for each sample werereconstructed from 3600 projection images.

Micro-XANES spectroscopy at the S K edge was performed on several keystones at the ID21 beamline of the European Synchrotron Radiation Facility in Grenoble, France. A 0.3 x 0.3 μm^2 beam of approximately 1E9 ph/s impinged on the keystones placed on a high resolution piezoelectric sample holder. A HpGe detector recorded the fluorescence signal at 90° with

respect to the beam. A Si photodiode placed before the sample recorded the fluorescence emitted by a thin Kapton or Al foil in order to monitor the incident intensity. A Si 111 double crystal monochromator was used to scan a region of 50 eV at the S K edge at 2.475 keV in steps of 0.3 eV. Several acquisitions were summed to insure good statistics and check for beam-induced redox. Scans of the track entry hole, middle of the track and a terminal grain were performed in order to estimate the redox state as a function of particle penetration into the aerogel.

Sample Modification and Contamination

All of the Wild 2 particles we have thus far examined have been modified, both physically and mineralogically, to various degrees by the capture process. All particles that may have been loose aggregates, "traveling sand piles", disaggregated into individual components with the denser components penetrating more deeply into the aerogel, and "outrunning" the most severely-heated aerogel at the front of the penetration tracks. Individual grains experienced a wide range of heating effects that range from excellent preservation to melting and total dissolution in >1200˚C molten aerogel. (Fig. 1). As a result of this heating many Fe-Ni sulfides have been melted (requiring ~1000˚C, ignoring pressure effects) (*S7*), have lost S due to partial evaporation, and are scattered among the Wild 2 samples as fine Fe-Ni-S beads with non-stoichiometric compositions, often intimately mixed with Fe-Ni metal. Such behavior was expected from our previous experience with silica aerogel and metals both in the laboratory and in actual use in low-Earth orbit (*S4, S8, S9*). The presence of these beads is an indicator that a particular component has been severely heated. What is remarkable is the extreme variability of these modifications and the fact that severely modified and unmodified materials can be found within a micrometer of each other, requiring tremendous local temperature gradients. Within a

single captured grain we can observe places where Fe-Ni sulfides have melted, partially devolatilized (loss of S), and mixed with Fe-Ni metal, whereas in other places we see survival of rather delicate Fe-Ni sulfide crystals. A fundamental problem is recognizing the modified grains for what they were prior to impact – discriminating between severely modified and relatively pristine mineral assemblages. Micro-XANES shows that at the beginning of Track 59, sulfate is present as well as an almost neutral S compound, which we believe to have formed during capture heating of sulfides.

Fortunately, we have an internal gauge of heating during collection. Fe-Ni sulfides are ubiquitous in the Wild 2 samples, are very sensitive indicators of heating, and accurate compositional analyses can reveal which have lost S, and which have not (and are therefore stoichiometric) (see Fig. 2a).

One unfortunate result of the fine-scale mixing of the Wild 2 grains with silica aerogel is that it is very difficult to obtain precise analyses for Si smaller than the thickness of ultramicrotomed sections, and any indigenous amorphous cometary materials are now hard to recognize amongst very abundant amorphous silica aerogel and melted cometary minerals. Any indigenous stoichiometric cometary materials are also so mixed, making their identification by purely chemical means very, very difficult. This is partially compensated by materials captured on the aluminum foils, where elemental ratios to Si can be measured, although these residues have undergone even higher pressure and temperature processing than in the aerogel.

Our initial hypothesis was that the degree of captured particle modification would vary considerably along each capture track, with the most modified material being present along the walls of the upper reaches of tracks, and the least modified situated at track termini. To test this idea we analyzed multiple (up to 53) grains from each of three long tracks (all exceeding 1 cm in

length). The results for the track with the most complete results (Track 35) are shown in Fig. S1. It is clear that crystalline grains are found along the entire track, not just at the terminus. While it is true that grains at track termini are generally dominated by crystalline material, these terminal grains are sometimes found to be large monomineralic fragments (sometimes single crystals) which have been fractured, disaggregated and thoroughly mixed with aerogel during capture. Because of this mixing, attempts to prepare samples by focused ion beams (FIBing) sometimes come to grief. While grains from the upper reaches of the tracks are universally disaggregated to some degree, many are dominated by materials that are still crystalline, including delicate Fe-Ni sulfides. Some terminal grains are found to be very fine-grained and polymineralic. Therefore one cannot sample a particular segment of any track with the certain expectation of finding only melted grains. Each track is different, and most contain unmelted samples along their entire length.

Several mineralogic contaminants have been introduced to the samples from trace impurities in the silica aerogel itself. These include materials from the aerogel manufacture process, handling before and during insertion into the Stardust grid, removal from the grid following flight, and sample removal from the aerogel cell. In addition, some of the earliest sample characterization work was performed on chips of aerogel found loose inside the Stardust canister immediately upon opening in the JSC Stardust clean room and were thus subject to additional contamination sources.

One such contaminant is calcite, present as sub-micrometer anhedral to euhedral grains with a composition, determined by STEM-EDX analyses, of pure $CaCO_3$, and the calcite structure confirmed by SAED patterns. These contaminants can usually be easily recognized as such by their occurrence external to the Wild 2 grains, situated instead in the enclosing shells of

compressed to melted aerogel. Calcite has been found principally in the loose chips of aerogel recovered from inside of the canister, where contamination opportunities were greatest. Given the importance of carbonates, this is a very unfortunate contaminant, but with careful observation it can be recognized easily as such and be discounted.

A more perplexing material is titanium oxide, usually present here as submicrometer-sized crystallites of brookite (TiO_2), but occasionally occurring as other titania phases, and sometimes containing Al_2O_3 and or Zr_2O_3. These materials usually found surrounding the Wild 2 grains, in enclosing aerogel, and also occasionally lying within the grains. It is therefore possible that a fraction of this material is indeed indigenous to the cometary material. However, these phases are common whitening agents in papers and spacecraft thermal control paints (*S10*) (though on the Stardust spacecraft none of these paints were in the line of sight of the aerogel), and their presence among the Wild 2 samples is a problem left to future resolution.

These minor exceptions aside, we found very limited contamination from the spacecraft in the aerogel. Potential problems with secondary impacts (cometary grains impacting on the spacecraft, ricocheting and splashing onto the aerogel) failed to materialize. Based on our experience, future missions should be able to avoid this problem almost entirely.

Track 25 - Comparison to CAI in CV3 and CM2 Chondrites

Some analyses of pyroxene from the one slice of the Track 25 terminal grain containing gehlenite fall within the range of typical Ti-, Al-rich clinopyroxene from CAIs in CV3 chondrites (e.g. Allende), termed “fassaite” (*S11*); the comparison would be stronger if we could measure the Ti^{3+}/Ti^{4+} ratio of the grain (Fig. S4). Compositions of pyroxenes from subparticles

and at least one other slice of the terminal particle, however, do not overlap with Allende compositions and do not exhibit the interelement covariations seen in meteoritic pyroxenes (Fig. S4). For example, Allende fassaite analyses (*S12*) define clear trends in which MgO is strongly correlated with SiO_2 and anticorrelated with TiO_2. (Fig. S4a&c). The Track 25 pyroxenes do not fall on these trends. The Track 25 pyroxenes have lower CaO contents than meteoritic CAI clinopyroxene, though there is some uncertainty in the interpretation of the analyses of some Wild 2 pyroxene due to possible contamination from adjacent phases, and the extrapolation of analyses from low count rates. Calculations in which possible excess silica (from the aerogel) and spinel (from the sample) components were removed from the Track 25 EDS analyses did not improve the fits to the Allende trends. Also, the Track 25 samples are much finer grained than most meteoritic CAIs, as were the few observed refractory IDPs (*S13, S14*). Overall, due to the differences in pyroxene composition trends, the presence of osbornite, and the apparent low abundance of melilite, the Track 25 sample does not appear to be identical to coarse-grained refractory inclusions from CV3 chondrites.

A better match for the mineralogy of the Track 25 grains would be the spinel-pyroxene inclusions found in CM2 chondrites such as Murchison, CR2 and CH-CB chondrites (*S15, S16, S17, S18, S19*). The CAI in CM chondrites tend to have spinel-rich cores and pyroxene-rich outer regions, which is what the Track 25 subgrains might represent. The pyroxene in them is aluminous and commonly contains Ti. Some spinel-rich inclusions in Murchison contain minor amounts of melilite, as does Track 25. Mg-Al spinel from refractory objects in Murchison is ^{16}O-rich, ~-40‰, but the O-isotopic composition of pyroxene in CM spinel-pyroxene inclusions is not known.

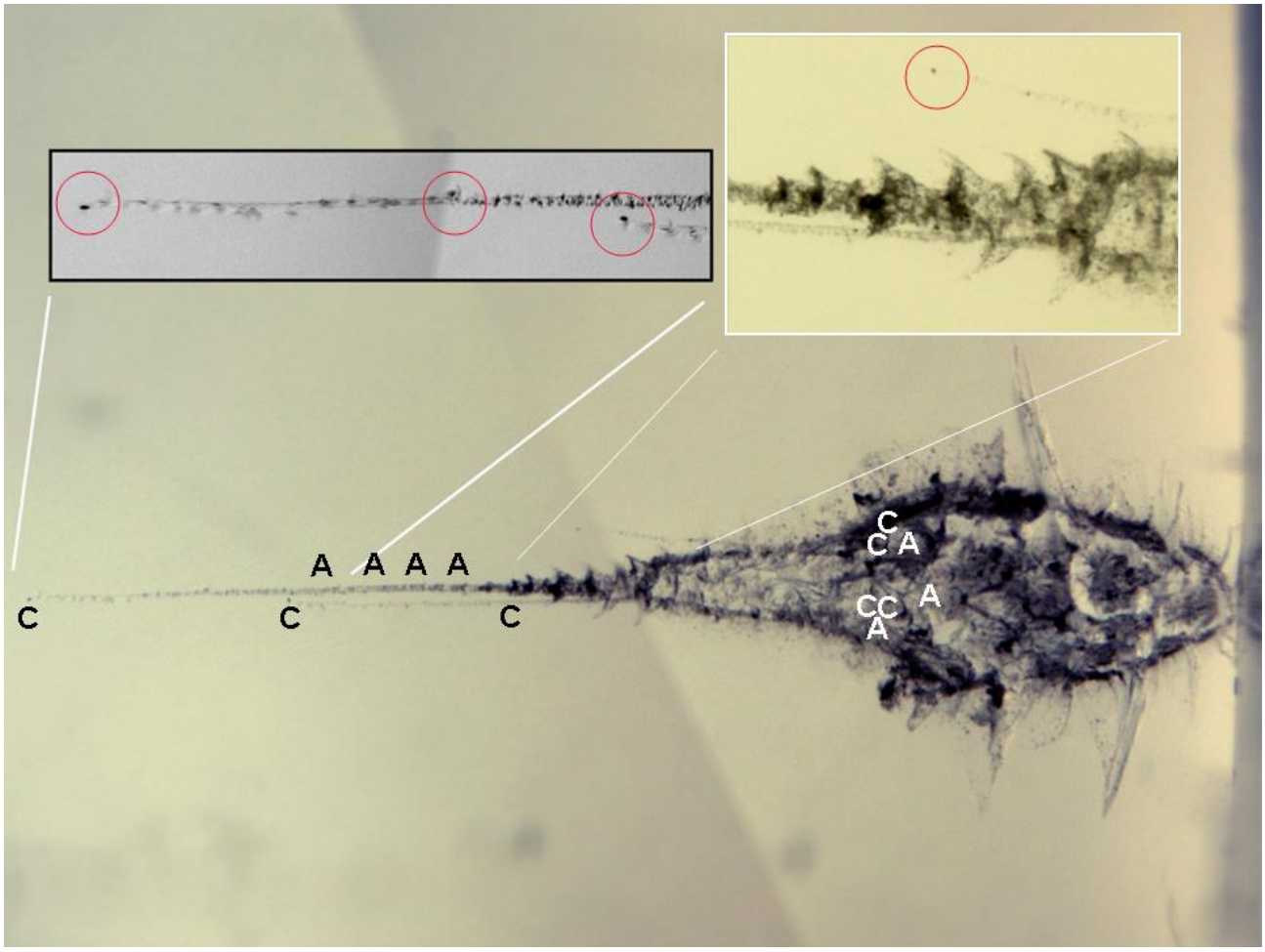

Figure S1. Results of crystallographic analyses of 14 grains removed from the length of Track 35, which is 11.7 mm long, and is shown here in transmitted light. The cometary particle entered the aerogel at the right, and traveled to the left. The location of predominantly crystalline fragments are indicated as “C”, those that are entirely amorphous are “A”. It is clear that crystalline fragments are located along most of the track.

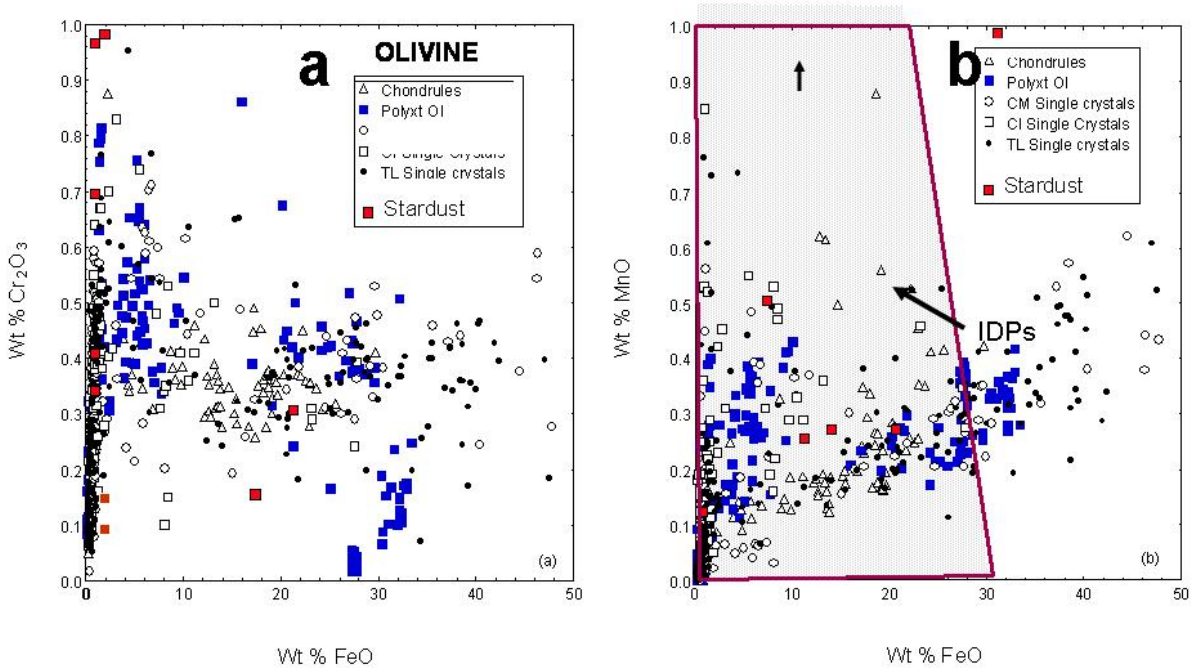

Figure S2. a: Cr and b: Mn contents of Wild 2 olivine compared with those in chondritic meteorites, including chondrules, polycrystalline aggregates (polyxt Ol), CM, CI and Tagish Lake (TL) single crystals (*S20*). Also shown is the MnO content of olivine in chondritic IDPs (*S21*). The analyses done thus far suggest that the composition field of the Wild 2 olivine is basically similar to all of these materials for the minor elements Mn and Cr.

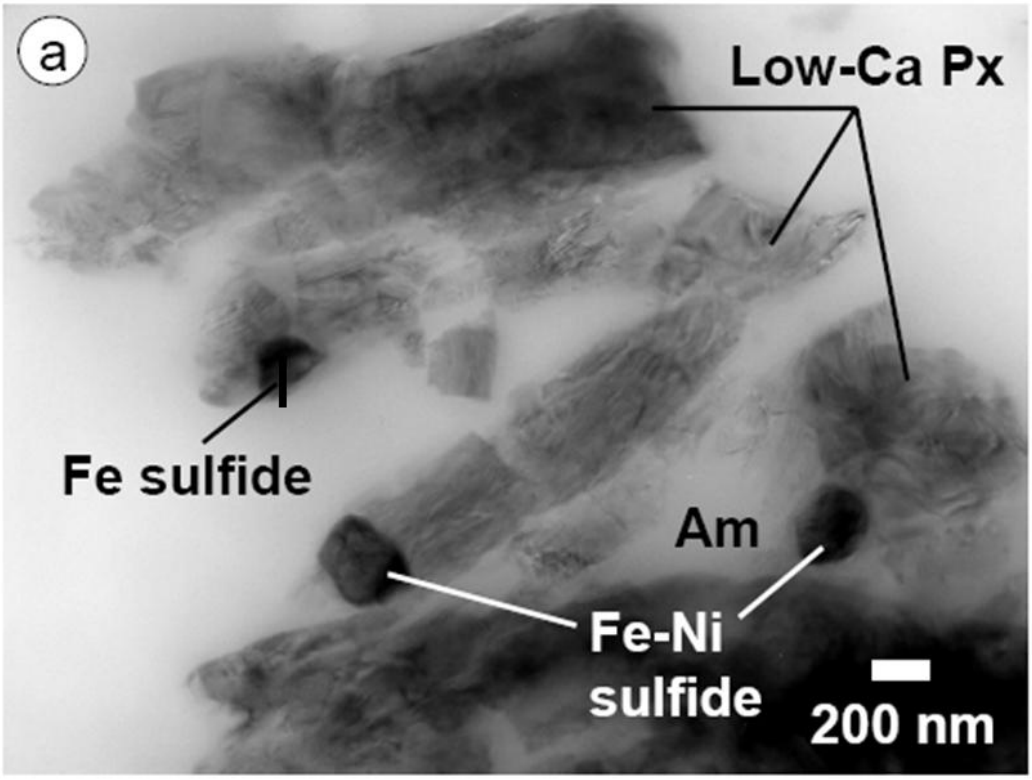

Figure S3. Bright field TEM image of abundant Fe-Ni sulfides scattered among low-Ca pyroxene and amorphous silicate material in the terminal grain from Track 17.

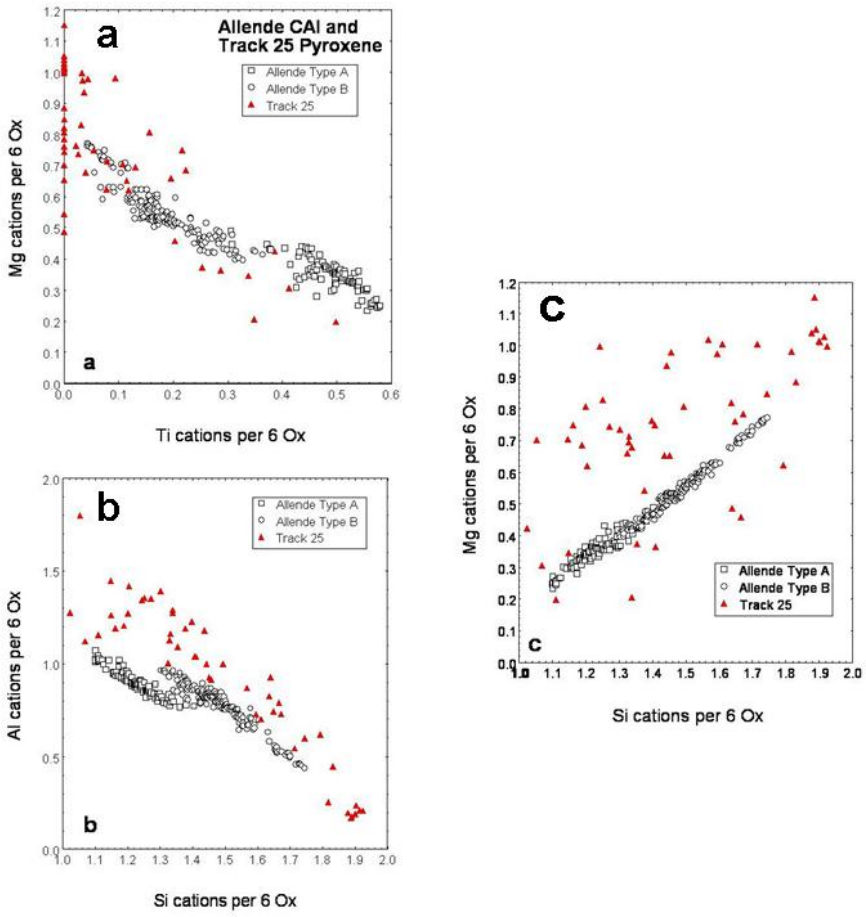

Figure S4. Compositional trends of fassaite in Allende CAIs compared with that for the Wild 2 Track 25 CAI-like grain, in terms of cations per six oxygen anions. a: Mg vs. Ti. Track 25 grains have a much weaker anticorrelation than the Allende fassaite. b: Al vs. Si. Track 25 grains have an anticorrelation like that of the Allende fassaite, but generally with a higher Al/Si ratio. c: Mg vs. Si. Track 25 grains do not exhibit the same correlation as the Allende fassaite. Allende data from (*S12*, *S22*, *S23*).

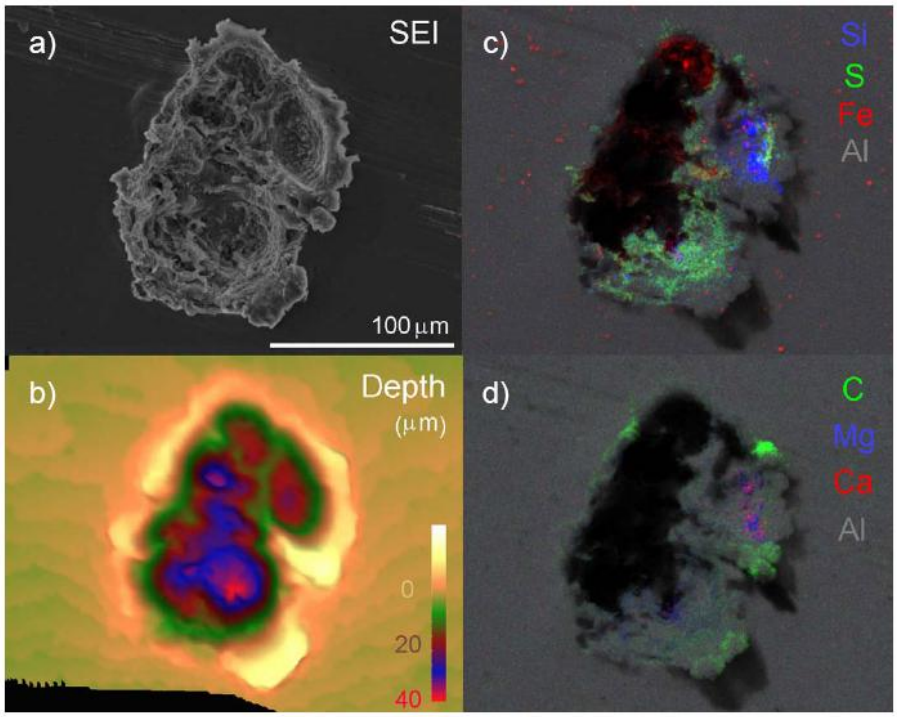

Figure S5. (a) Secondary electron image of a complex crater preserved in foil C2029W,1. The crater contains several mass centers suggesting the original cometary projectile was aggregated. (b) A depth gradient map for the crater. (c&d) Composite energy-dispersive X-ray elemental maps showing the distribution of the different remnant mineral phases preserved in the crater (e.g. silicate and sulfide).

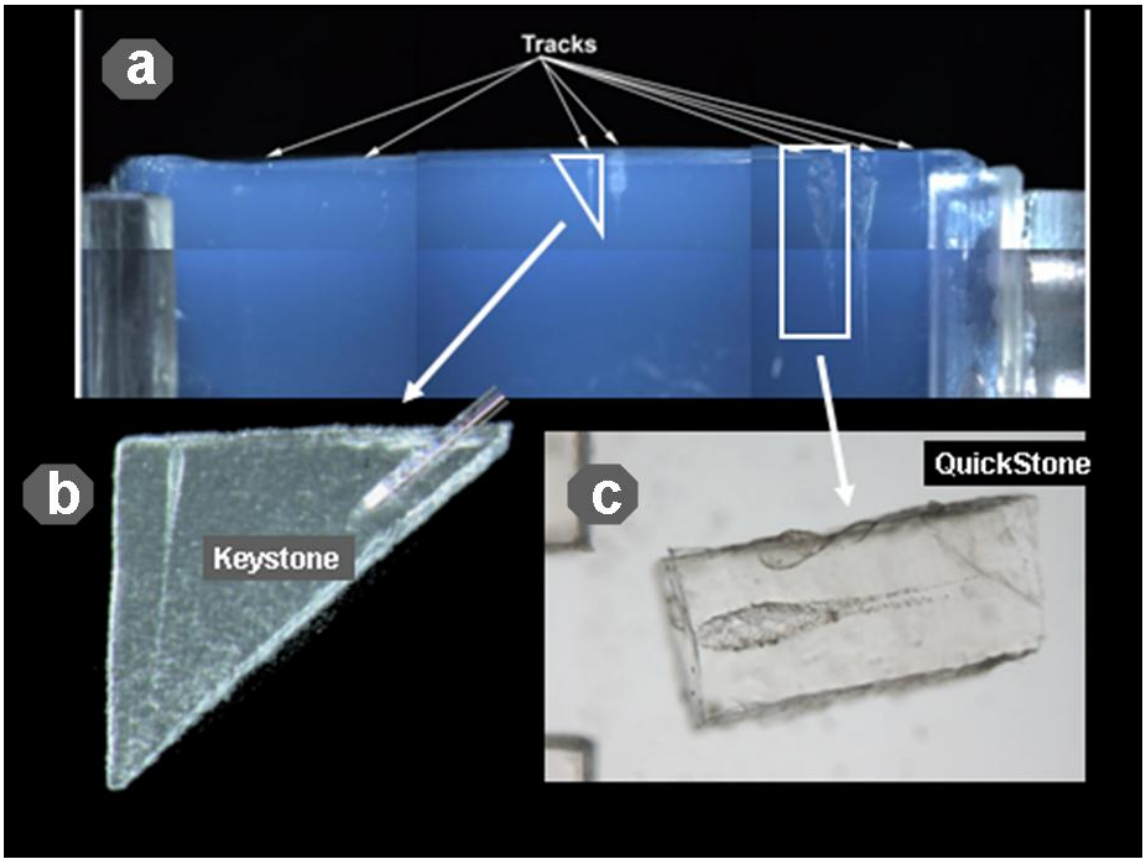

Figure S6. Two particle extraction techniques developed for aerogel. a: Side view of a complete cometary aerogel cell, containing numerous tracks. Outlines indicate the location of a keystone and quikstone to be removed. b: Triangular keystone, removed from aerogel with a track visible within. This keystone measures approximately 3 mm in length. c: Quikstone parallelepiped containing a large bulb-type track. The track measures approximately 1 cm in length.

References and Notes

S1. http://curator.jsc.nasa.gov/stardust/sample_catalog/index.cfm.

S2. A.J. Westphal et al., *Meteoritics & Planetary Science* 39, 1375 (2004).

S3. H.A. Ishii, G.A. Graham, A.T. Kearsley, P.G. Grant, C.J. Snead, J.P. Bradley, *MAPS* 40, 1741(2005).

S4. R.A. Barrett, M.E. Zolensky, F. Hörz, D.J. Lindstrom, E.K. Gibson, *Proceedings of the 19th Lunar and Planetary Science Conference*, 22, 203 (1992).

S5. T. Stephan, *Planet. Space Sci.* 49, 859 (2001).

S6. K. Uesugi, A. Takeuchi, Y. Suzuki. *Proceedings of SPIE* 6318, (2006).

S7. D. Vaughan, J. Craig, *Mineral Chemistry of Metal Sulfides*. Cambridge Univ. Press., 493 (1978).

S8. F. Hörz, M.E. Zolensky, R.P. Bernhard, T.H. See, J.L. Warren, *Icarus* 147, 559 (2000).

S9. M.J. Burchell, G. Graham, A. Kearsley, *Annual Review of Earth and Planetary Sciences* 34, 385 (2006).

S10. M.E. Zolensky, D. S. McKay, L. A. Kaczor *Journal of Geophysical Research* 94, D1, 1047 (1989).

S11. E. Dowty, J.R. Clark , *American Mineralogist* 58, 230 (1973).

S12. S.B. Simon, L. Grossman, *Geochimica et Cosmochimica Acta 70*, 780 (2006).

S13. M.E. Zolensky, *Science* 237, 1466 (1987).

S14. K. McKeegan, *Science* 237, 1468 (1987).

S15. G.J. MacPherson, M. Bar-Matthews, T. Tanaka, E. Olsen, L. Grossman, *Geochim. Cosmochim. Acta* 47, 823 (1983).

S16. G.J. MacPherson et al., *Proc. 15th Lunar Planet. Sci. Conf., JGR* 89, supplement, C299 (1984).

S17. J. Aléon, A.N. Krot, K.D. McKeegan, *Meteoritics Planetary Science* 37, 1729 (2002).

S18. M.K. Weisberg, M. Prinz, C.E. Nehru, *Earth and Planetary Science Letters* 91, 19 (1988).

S19. A.N. Krot, M. Chaussidon, G.R. Huss, A.A.Ulyanov, M.A. Ivanova M. A., *Meteoritics and Planetary Science* 41, A101 (2006).

S20. S.B. Simon, L. Grossman, *Meteoritics Planetary Science* 38, 813 (2003).

S21. W. Klöck, K.L. Thomas, D.S. McKay, H. Palme, *Nature* 339, 126 (1989).

S22. S.B.Simon et al., *Geochimica et Cosmochimica Acta* 55, 2635 (1991).

S23. S.B.Simon et al., *Geochimica et Cosmochimica Acta* 63, 1233 (1999).